






# Exploring Intercellular Dynamics: Ultra-Weak Biophoton Emission as a Novel Indicator of Altered Cell Functions and Disease in Oligospermia Mice

Arefeh Aryan<sup>1,2#</sup>, Fakhroddin Aghajanpour<sup>1,3#</sup>, Masoomeh Dashtdar<sup>4</sup>, Fatemeh Hejazi<sup>5</sup>, Maryam Salimi<sup>3</sup>, Azar Afshar<sup>3</sup>, Reza Soltani<sup>3</sup>, Ahad Hasan Seyed Hasani<sup>3</sup>, Abbas Aliaghaei<sup>3</sup>, Hojjat-Allah Abbaszadeh<sup>1</sup>, Hasan Mahmoodi<sup>4</sup>, Leila Zahedi<sup>6</sup>, Mohammad-Amin Abdollahifar<sup>1,3#</sup>, Fatemeh Fadaei Fathabadi<sup>1,3#</sup>

<sup>1</sup>Laser Application in Medical Sciences Research Center, Shahid Beheshti University of Medical, Sciences, Tehran, Iran

<sup>2</sup>Anatomy Department, School of Medicine, Rasht University of Medical Sciences, Gilan, Iran

<sup>3</sup>Department of Biology and Anatomical Sciences, School of Medicine, Shahid Beheshti University of Medical Sciences, Tehran, Iran

<sup>4</sup>Department of Physics, Shahid Beheshti University, Tehran, Iran

<sup>5</sup>Department of Advanced Technology, Shiraz University, Shiraz, Iran

<sup>6</sup>Department of Physical Electronics, Faculty of Science, Masaryk University, Brno, Czech Republic

## \*Correspondence to:

Mohammad-Amin  
Abdollahifar,  
Email: [m\\_amin58@yahoo.com](mailto:m_amin58@yahoo.com),  
[abdollahima@sbmu.ac.ir](mailto:abdollahima@sbmu.ac.ir) and  
Fatemeh Fadaei Fathabadi,  
Email: [fatemeh.fadaeifathabadi@gmail.com](mailto:fatemeh.fadaeifathabadi@gmail.com)

<sup>#</sup>These two first authors  
contributed equally to this  
work.

Received: August 9, 2023  
Accepted: November 12, 2023  
ePublished: December 26, 2023



## Abstract

**Introduction:** Biophoton emission, the spontaneous release of photons from living cells, has emerged as an attractive field of research in the study of biological systems. Scientists have recently discovered that changes in biophoton emission could serve as potential indicators of pathological conditions. This intriguing phenomenon suggests that cells might communicate and interact with each other through the exchange of these faint but significant light signals. Therefore, the present study introduces intercellular relationships with biophoton release to detect normal and abnormal cell functions to further achieve cellular interactions by focusing on cell and cell arrangement in disease conditions.

**Methods:** Twenty male mice were assigned to control and busulfan groups. Five weeks after the injection of busulfan, the testis was removed, and then the stereological techniques and TUNEL assay were applied to estimate the histopathology of the testis tissue sections.

**Results:** The findings revealed that the ultra-weak biophoton emission in the control group was significantly lower than in the busulfan group. The oligospermia mice model showed that it significantly changed the spatial arrangement of testicular cells and notably decreased the testis volume, length of seminiferous tubules, and the number of testicular cells. The results of the TUNEL assay showed that the percentage of apoptotic cells significantly increased in the busulfan group.

**Conclusion:** The ultra-weak biophoton emission from testis tissue was reduced in oligospermia mice. As a result, the decline of ultra-weak biophoton can indicate a change in cell arrangement, a decrease in intercellular interaction, and eventually disease.

**Keywords:** Photon emission; Spatial arrangement; Spermatogenesis; Apoptosis.

## Introduction

Cellular communication and interactions are fundamental processes in the organization, development, and maintenance of multicellular organisms.<sup>1,2</sup> The coordinated functioning of cells within a complex system relies on intricate signaling mechanisms that facilitate intercellular communication.<sup>2,3</sup> An understanding of these mechanisms is crucial for unraveling the physiological and pathological conditions that govern cellular behaviors.<sup>3</sup> Recently, the concept of biophoton emission has emerged as a potential indicator of cellular interactions and pathological states.<sup>4</sup> This phenomenon

suggests that cells communicate with each other through the exchange of ultra-weak light signals, providing a novel perspective on intercellular communication.<sup>4</sup>

However, despite the growing interest in biophoton emission and its potential implications, there exists a notable gap in the current research literature. Specifically, prior studies have primarily focused on describing the phenomenon and its association with various physiological and pathological conditions. Yet, there is a distinct lack of comprehensive investigations into the intricate relationships between cellular arrangements, intercellular communication, and biophoton emission,

especially concerning pathological conditions. This gap in knowledge represents a critical area for further exploration.

Cellular interactions are essential for the proper functioning of multicellular organisms. These interactions orchestrate various processes, including embryogenesis, cancer metastasis, differentiation, diabetes, and immunological responses.<sup>1,5</sup> Through the expression of ligand molecules and cell surface receptors, cells establish intercellular arrangements that enable communication and coordination of their activities.<sup>5,6</sup> Signaling molecules play a crucial role in conveying information between cells, ensuring their proper functioning and tissue development.

Biophoton emission, an intriguing aspect of cellular communication, has gained attention in recent years. Ultra-weak biophoton emission refers to the extremely faint light emitted by living organisms due to their metabolic activities.<sup>7</sup> This emission arises from photochemical reactions and electromagnetic field interactions within cells, extending beyond traditional signaling mechanisms.<sup>8,9</sup> Studies have demonstrated the existence of non-thermal electromagnetic waves and photons emitted by cells in the visual range, suggesting their involvement in cellular interactions.<sup>8,9</sup>

Notably, variations in biophoton emission have been observed in different physiological and pathological contexts. For instance, changes in biophoton emission have been correlated with physical injury, exposure to toxins, and cell division.<sup>10,11</sup> These findings highlight the potential of biophoton emission as an indicator of cellular states, including pathological conditions. Consequently, exploring the relationship between biophoton emission and cellular interactions could offer valuable insights into disease detection and understanding of abnormal cell functions.

In light of the importance of cellular interactions and the potential significance of biophoton emission, this study aims to investigate the intricate relationships between cellular arrangements, intercellular communication, and biophoton emission in the context of pathological conditions. By comprehensively analyzing existing research and experimental evidence, we seek to shed light on the diagnostic applications of biophoton emission and its role in unraveling the complex web of cellular interactions. The findings of this study may pave the way for new insights into cellular functions, disease detection, and personalized medicine.

Therefore, by elucidating these aspects, we aim to contribute to our understanding of cellular interactions and their connection in oligospermia induced by busulfan as compared with normal states.

## Materials and Methods

### Animals

From the laboratory animal center, 20 male adult NMRI mice (27-30 g) were selected for the current study. The mice were housed in standard conditions with access to water and food. There were two experimental groups of mice (10 mice each): I. A control group (C) consists of intact animals, and II. The mice were treated with busulfan (B) (45 mg/kg, single dose) for 35 days. After administering an intraperitoneal injection of 45 mg/kg, the mice were euthanized via cervical dislocation for subsequent assessments.<sup>12</sup>

### Ultra-Weak Photon Emission Measurements

A photomultiplier tube (PMT) (Hamamatsu H10722-01), [H10722\_TPMO1063E], was employed to measure the biophotons emitted from the samples. The PMT has a spectral response range of 230 nm to 870 nm and the maximum response at 400 nm. The gate time for collecting the photon signal was set at 1 second. The PMT worked at room temperature. The outputs of the PMT were recorded by National Instrument Data Acquisition (NI-DAG USB 6009) using LabVIEW software. The PMT and the sample were stored in a dark room to maintain optimum performance, and the power supply and the rest electronic setup were located outside the dark room. The samples were placed in a diameter polystyrene petri dish at a distance of about 3cm from the PMT input window.<sup>13</sup>

### Tissue Preparation

Bouin's Solution was applied overnight to the testicles. In each sample, using hematoxylin & eosin (H&E) (Sigma, USA) staining, 10 sections were selected by systematic uniform random sampling (SURS). Testicular cells were morphologically different for counting purposes.

### Volume (mm<sup>3</sup>) of Testis and Interstitium

To evaluate testis volume (mm<sup>3</sup>) and volume (mm<sup>3</sup>) of interstitial tissue, Cavalieri's principle was used<sup>14</sup>:

$$V_{total} = \sum P \times \frac{a}{P} \times t$$

( $\sum P$ ) represents the sum of falling points on the sections of testis tissue, ( $a/p$ ) represents the area of individual points, and ( $t$ ) is the distance between sample points.

### The Length of the Seminiferous Tubules (/mm<sup>2</sup>)

Using the following formula, seminiferous tubule length density/mm<sup>2</sup> was also estimated:

$$L_v = \frac{2 \sum Q}{\sum P \times \frac{a}{f}}$$

The total number of seminiferous tubules is  $\sum Q$ . The area per counting frame size is  $a/f$ , and the total number of microscopic fields is  $\sum P$ .<sup>14</sup>

### Number of Testicular Cells

Testicular cell numbers were estimated using optical



dissectors.<sup>14</sup> Based on the equation below, we calculated the numerical density ( $N_v$ ) of testis cells:

$$N_v = \frac{\sum Q}{\sum P \times h \times \frac{a}{f}} \times \frac{t}{BA}$$

( $\sum Q$ ) is the number of cells and ( $\sum P$ ) is the total number of microscopic fields; ( $a/f$ ) is the area per counting frame size; ( $h$ ) is the dissector height; ( $BA$ ) is the thickness of the microtome section and ( $t$ ) is the section's real thickness. Here is the formula for calculating the total testicular cells:

$$N_{total} = N_v \times V$$

### Johnsen Score

According to the Johnsen score, tissue sections were categorized based on their histopathological pattern. The process of spermatogenesis was evaluated on each slide using 100 tubules (Table 1).<sup>15</sup>

### Voronoi tessellation

Cells are represented by polygon regions. An area was drawn around each testicular cell using the ImageJ Voronoi Plugin. Testicular tissue microscopic images, along with an objective lens of 40 mm, were used to determine the closest Voronoi polygon to the testis and its area. "ImageJ" was then used to analyze the data. The variability of a polygonal region could easily be calculated by its variance. A testicular cell distribution can be determined by the coefficient of variation (CV, mean x 100, standard deviation of polygonal regions). There is a random distribution of testicular cells in CV 33 to 64%. More than 64% of CVs have a cluster distribution, while less than 33% have a regular pattern. Rather than a statistical comparison, this CV is a classification.<sup>16</sup>

### Coefficient of Error (CE)

The following equation was used to calculate CE (V):

$$CE(V) = (\sum P^{-1}) \times 1/2$$

According to the equation below,<sup>14</sup> CE is calculated for testicular volume and testicular cells:

$$CE(N) = [CE^2(N_v) + CE^2(V)]^{1/2}$$

$$CE(N_v) = \left[ \left( \frac{n}{n-1} \right) \times \left[ \left( \frac{\sum(Q)^2}{(\sum Q)^2} \right) + \left( \frac{\sum(P)^2}{(\sum P)^2} \right) - \left( \frac{2\sum(QP)}{\sum Q \sum P} \right) \right] \right]^{1/2}$$

### Covariance Function

The following equation was used to measure the covariance function<sup>17-20</sup>:

$$C(r)X = \frac{\sum DP(XYr)}{\sum DP(refr)}$$

The class size of both dipole endpoints (DP) was  $r = 1$  (4.3 m).  $V_v$ ,  $C(r)$ , and  $g(r)$  were estimated using distances (DP) between 0 and 49. Therefore, there was 210.7 m ( $52.9 \times 4.3 = 210.7$  m).

### Pair Correlation Function

Normalized covariance is determined by dividing the covariance by the reference value (squared volume fraction), which is described by the pair correlation function<sup>17-19, 21</sup>:

$$g(r) = \frac{C(r)}{V_v^2}$$

### Cross-covariance Function

To quantify spatial arrangement ( $C(r)X, Y$ ), cross-covariance is used. The formula below can be used to calculate it<sup>17-19, 21</sup>:

$$C(r)X = \frac{\sum DP(XYr)}{\sum DP(refr)}$$

### Cross-correlation Function

For volume fraction differences to be eliminated, we need to normalize the cross-covariance using the formula below<sup>17-19, 21</sup>:

$$g(r)XY = \frac{C(r)XY}{V_v(Xref) \times V_v(Yref)}$$

### TUNEL Assay

To determine the percentage of apoptotic cells, the TUNEL assay (In-Situ Cell Death Detection Kit, POD; Roche) was performed. On poly-l-lysine-coated slides, testis tissue sections (5  $\mu$ m) were mounted and deparaffinized. 50 ml of an incubation solution (10–20 mg/mL) reacted with 50 mL of the TUNEL reaction mixture in a dark, humidified chamber after incubating tissue sections with proteinase K solution for 30 minutes. 3-amino-9-ethyl carbazole (AEC) was applied to tissue sections after washing in PBS.

**Table 1.** Histopathological Classification of Testicular Tissue According to the Johnsen Score

Score	Level of Spermatogenesis
10	Full spermatogenesis
9	Slightly impaired spermatogenesis
8	Less than five spermatozoa per tubule
7	No late spermatids; many early spermatids
6	Few early spermatids; arrest of spermatogenesis at the spermatid stage
5	Many spermatocytes
4	Few spermatocytes, arrest of spermatogenesis at the primary spermatocyte stage.
3	Spermatogonia only
2	No germ cells, Sertoli cells only
1	No seminiferous epithelial cell, tubular sclerosis

Hematoxylin was then used to counterstain the sections. Apoptotic testicular cells were defined as cells with brown nuclei if TUNEL-positive cells were quantified.

**Statistical Analyses**

Quantitative data were represented as mean ± SD. Kolmogorov–Smirnov tests indicated that all quantitative data followed a normal distribution. Consequently, we employed t-tests for data analysis, utilizing SPSS software version 21.00 (IBM Corp., Armonk, NY, USA). A significance threshold of  $P \leq 0.05$  was applied to all data.

**Results**

**Ultra-weak Photon Emission Measurements**

In all recorded ultra-weak photon emission measurements, the background noise level was measured and subtracted from the recorded ultra-weak photon emission. The recorded ultra-weak photon emission from the control group in a detection time of 5 min. is presented in Figure 1. Statistical comparison of the results showed that the recorded ultra-weak photon emission from the control ( $0.511 \pm 0.301$ ) group was significantly different in comparison to the busulfan ( $0.222 \pm 0.051$ ) group in a detection time of 5 min ( $P = 0.046$ ). Figure 1 indicates that induced oligospermia in mice by busulfan is associated with a decrease in the integrated ultra-weak photon emission.

**Stereological Studies**

Based on stereological results, the total volume ( $\text{mm}^3$ ) of the testicle and the length of seminiferous tubules ( $/\text{mm}^2$ ) significantly decreased in the busulfan ( $12.13 \pm 2.21$ ) ( $2119.7 \pm 259.39$ ) group compared to the control ( $21.66 \pm 1.27$ ) ( $3578.7 \pm 118.67$ ) group ( $P = 0.00$ ), respectively (Figure 2A and B). As shown in Figure 3A-E, the number of spermatogonia, primary spermatocytes, round spermatids, Sertoli, and Leydig cells significantly decreased in the busulfan ( $5.95 \times 10^6 \pm 1.72 \times 10^6$ ) ( $7.97 \times 10^6 \pm 1.55 \times 10^6$ ) ( $18.25 \times 10^6 \pm 3.57 \times 10^6$ ) ( $18.05 \times 10^3 \pm 1.74 \times 10^3$ ) ( $7.73 \times 10^3 \pm 0.74 \times 10^3$ ) group compared to the control ( $18.65 \times 10^6 \pm 0.79 \times 10^6$ ) ( $27.64 \times 10^6 \pm 1.53 \times 10^6$ ) ( $54.44 \times 10^6 \pm 2.68 \times 10^6$ ) ( $23.99 \times 10^3 \pm 1.63 \times 10^3$ ) ( $18.15 \times 10^3 \pm 1.65 \times 10^3$ ) group ( $P = 0.00$ ), respectively.

**Histopathological Analysis**

The overall histopathological findings showed normal spermatogenesis in the control group. As illustrated in Figure 4A and B, the injection of busulfan with a dose of 45 induced severe degenerative alterations resulting in the entire depletion of some seminiferous tubules from cells. However, there was a significant difference between the control ( $10 \pm 0.00$ ) group and the busulfan ( $7.83 \pm 0.75$ ) group ( $P = 0.00$ ) (Figure 4C).

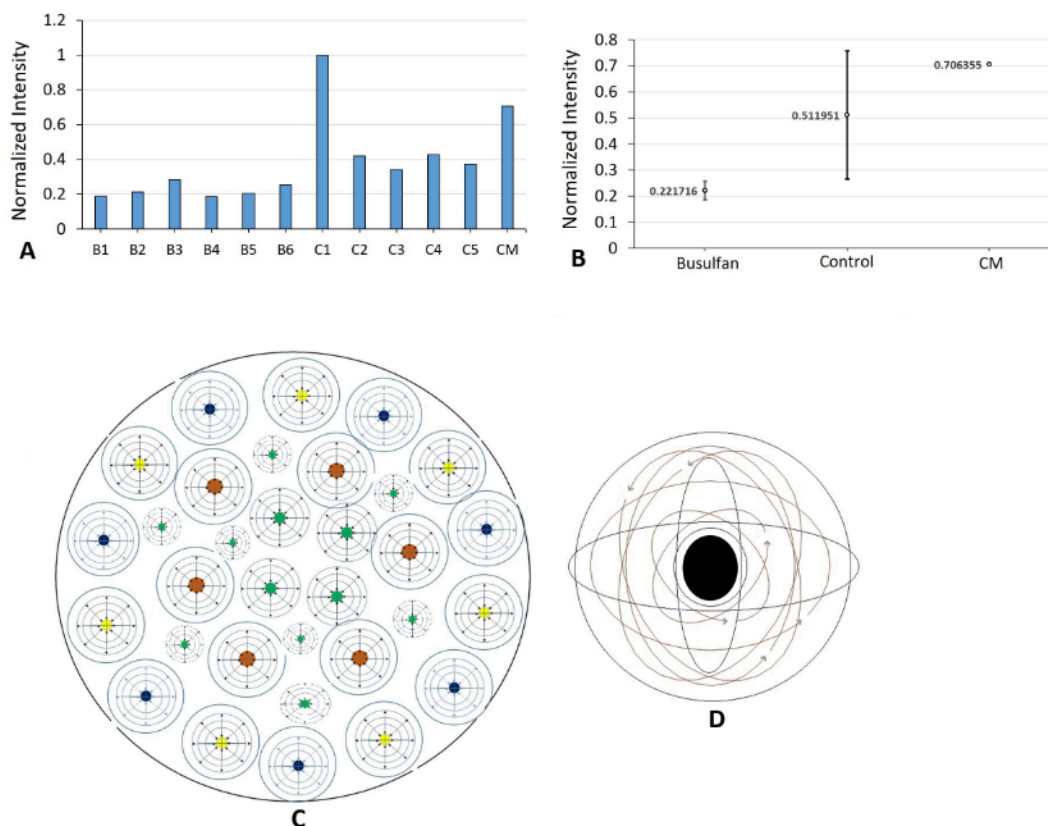


**Figure 1.** Ultra-weak photon emission. (A-C) Recorded ultra-weak photon emission from testis tissue in the control and busulfan groups in a detection time of 5 min (\*\* $P < 0.0001$ ). (D and E) A schematic diagram to show the electromagnetic field around testicular cells



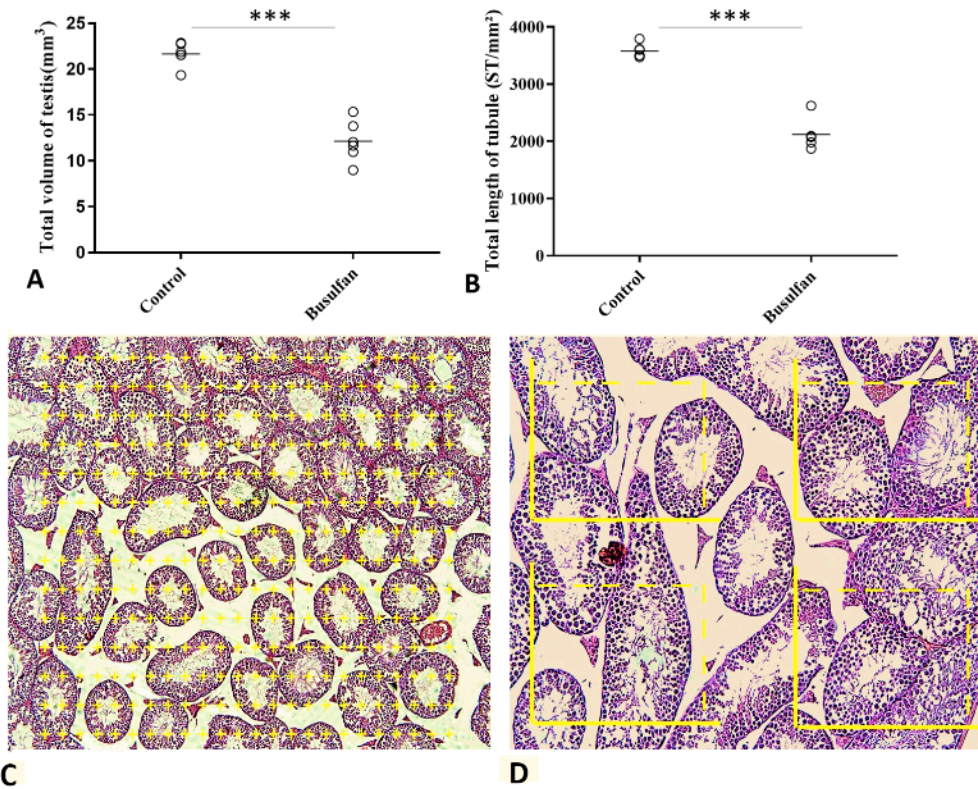


**Figure 2.** Testis volume and length of seminiferous tubules. (A and B) Mean  $\pm$ SD of the total testis volume and length of seminiferous tubules in the study groups ( $***P < 0.001$ ). (C and D) Photomicrograph of the testis stained with H&E. A point grid and counting frame are superimposed over the photomicrograph for measuring the volume of the testis and the length of seminiferous tubules (ST)

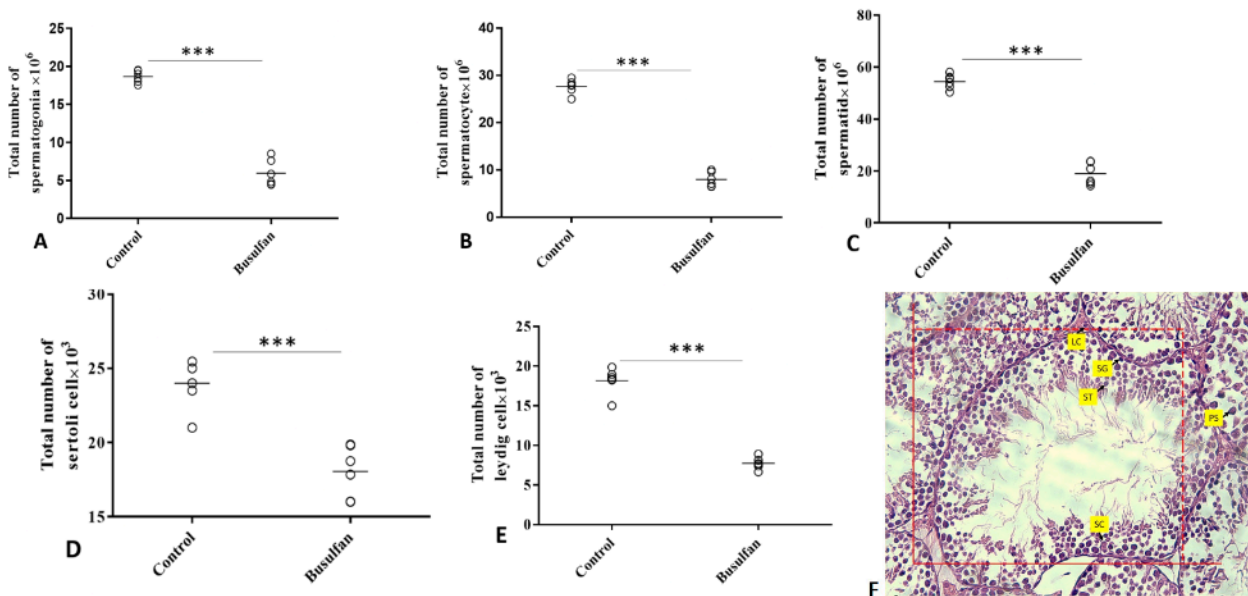


**Figure 3.** Total number of testicular cells. (A-E) Mean  $\pm$ SD of the total number of testicular cells in the study groups ( $***P < 0.001$ ). (F) Photomicrograph of the testis stained with H&E, 40X. Spermatogonia (SG), primary spermatocyte (PS), spermatid (ST), Sertoli cell (SC), Leydig cell (LC)

**The Spatial Distribution of the Testicular Cells**

Voronoi tessellations of testicular cells were shown in both the control group and the busulfan group (Figure 5A-E). In the busulfan samples, 70% of the polygons of the testicular cells in the testis were located between 120 and 130  $\mu\text{m}^2$ . In the control samples, only 45% were within  $<120 \mu\text{m}^2$ . Busulfan samples also showed that 20% of the

testicular polygons were located within the range of 120-130  $\mu\text{m}^2$ , in contrast to just 32% of the control samples. In addition, in the busulfan samples, 10% of the areas of the polygons of these cells were within  $<130 \mu\text{m}^2$ , while in the control samples, only 22% of these areas were within this size range. Further, the busulfan samples showed a lower number of testicular cells in the 120-130

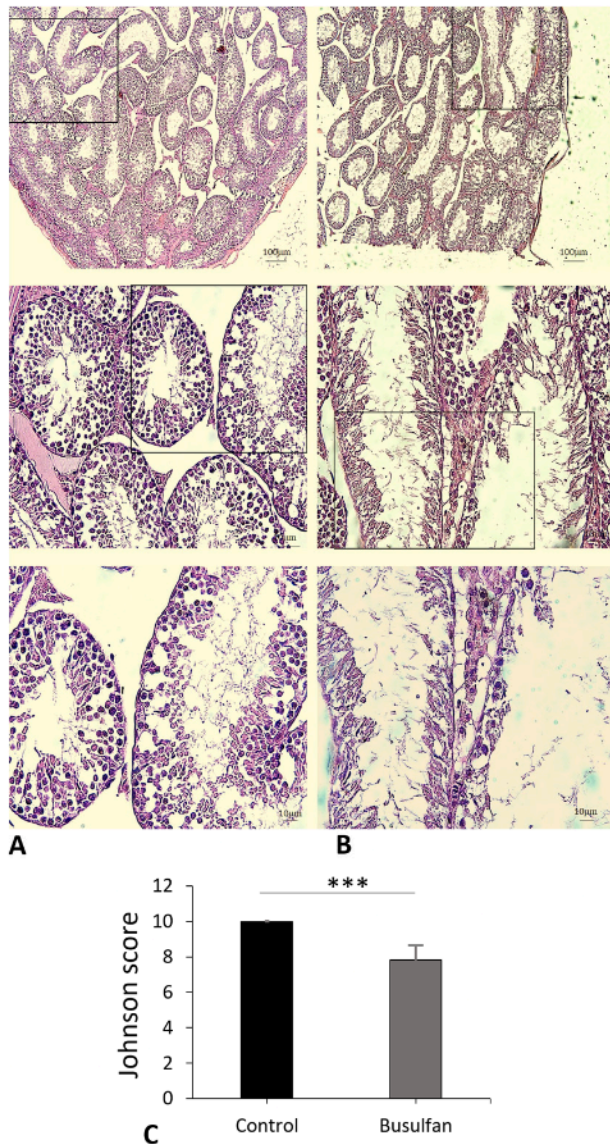


**Figure 4.** Johnson score. (A and B) Photomicrograph of the testis stained with H&E (4X, 10X, and 40X). (A) The histopathological findings showed normal spermatogenesis in all control autopsies, and the Johnson score was 10. (B) Testicular histopathology in the oligospermia mice induced by busulfan had some tubules with slightly impaired spermatogenesis, some with less than five spermatozoa per tubule, some with no late spermatids and many early spermatids, and some tubules with few early spermatids. (C) Mean  $\pm$  SD of the Johnson score in the study groups (\*\*\*)  $P < 0.001$

$\mu\text{m}^2$  (Figures 5A-E). A high degree of variation (CV) was observed in both groups based on the coefficient of variation classification ( $<33\%$ ) (Figure 5A-E).

#### Spatial Arrangement of Testicular Cells

Figure 6A-D shows the correlation functions for pair correlation functions and cross-correlation functions for testicular cells as a function of dipole distance ( $r$ ). There were significant differences between the busulfan and control groups in all of the graphs. Busulfan-induced mice's testicular cells had wider gaps, according to the results. Both groups' data points were randomly arranged after the gap at greater distances. An inverse correlation

is represented by a cross-covariance lower than the line. Busulfan has a negative effect on the correlation between testicular cells in the oligospermia mice (Figure 7A-E), whereas this correlation is positive in the control mice.

#### Percentage of apoptotic cells

Cell apoptosis was determined using a TUNEL kit. TUNEL-positive cell counts illustrated a considerable increase in the apoptotic cells in the busulfan group ( $78.8 \pm 7.8$ ) compared to the control group ( $12.4 \pm 0.8$ ) ( $P = 0.00$ ) (Figure 8A-C).

#### Discussion

In this study, we introduced a novel approach to evaluating the spatial arrangement of cells and its relationship with biophoton emission in healthy mice and a busulfan-induced oligospermia mice model.<sup>11,22-24</sup> Our findings are in line with previous research, suggesting a correlation between changes in biophoton emission and disruptions in the spatial arrangement of testicular cells in the oligospermia mice model. Specifically, we observed a significant reduction in ultra-weak photon emission from the busulfan-induced oligospermia mice, alongside a decrease in testis volume, seminiferous tubule length, and the number of testicular cells. Furthermore, our Johnson score results indicated severe degenerative changes in seminiferous tubules, indicative of oligospermia.

The spatial arrangement of testicular cells was assessed by using Voronoi tessellation and second-order stereology, revealing notable changes related to both biophoton emission and impaired spermatogenesis in the busulfan group. These changes may be attributed to impaired cell mitosis and meiosis in male germ cells. Importantly, the Voronoi tessellation technique demonstrated a distinct spatial distribution of testicular cells in the busulfan-induced mice. Our results strongly support the idea that ultra-weak photon emission decreases in response to heightened cell death in testicular cells observed in the oligospermia groups.

Our study assessed the condition 35 days after inducing oligospermia, rather than immediately after induction. This temporal aspect is significant, for we aimed to measure photon emission as an indicator of cellular activity. Our findings indicated a decrease in photon emission in oligospermia mice, contrasting the expected increase seen during acute phases or inflammation due to elevated ROS production.<sup>4,11,25</sup> This reduction is likely due to apoptosis initiating changes in cell spatial arrangement and tissue architecture, subsequently decreasing communication between testicular cells. The known effects of busulfan on DNA structure, spermatogonial stem cell proliferation, and cellular structural components are aligned with these findings, supporting the link between cellular function and activity.<sup>26,27</sup>

Although mitochondria are known to generate the



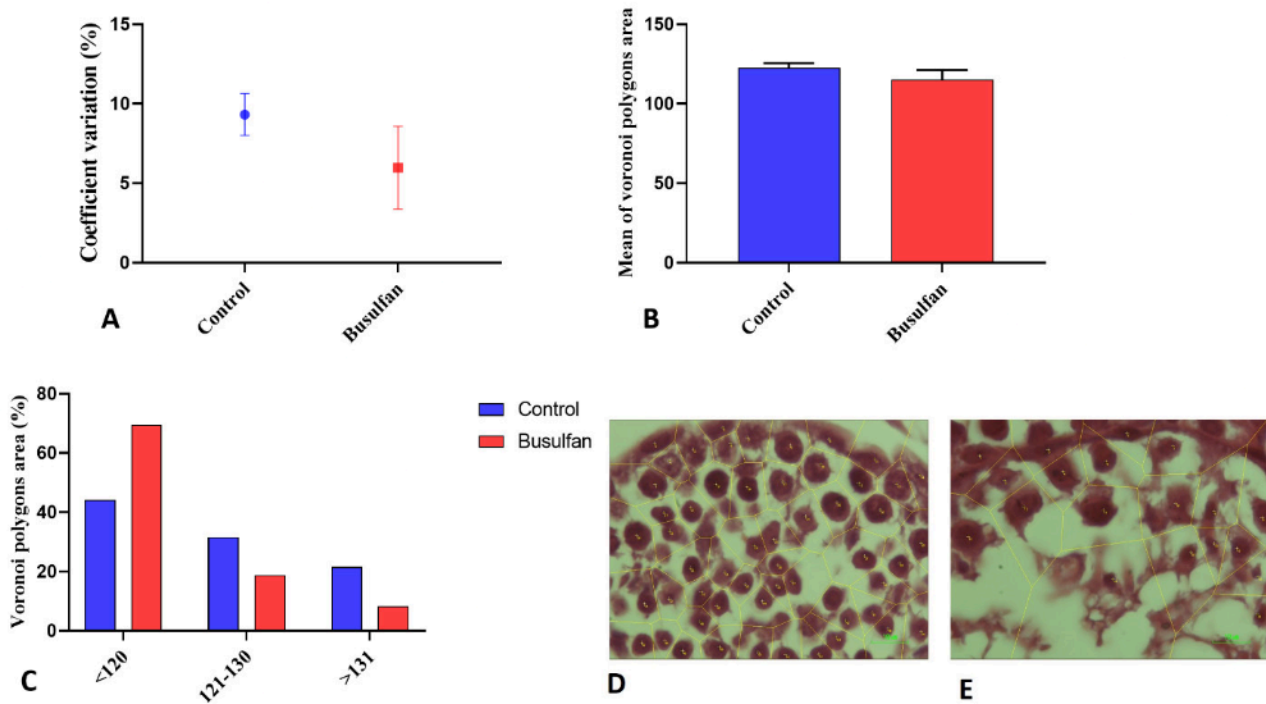


**Figure 5.** Evaluation of the Spatial Pattern of Testicular Cells Using Voronoi Tessellation. (A-C) Mean  $\pm$  SD and Coefficient of Variation (CV) of Voronoi polygon area (%) within the testis in the study groups. (D and E) Representative photograph, polygon area, and schematic of Voronoi tessellation of the testicular cells in the control (D) and busulfan (E) groups

majority of ultra-weak photon emissions, our results suggested a reduction in emission due to heightened cell death in the oligospermia groups.<sup>28</sup> While previous research has linked ultra-weak photon emission to ROS production, our study highlights a different outcome, emphasizing cellular communication.<sup>27</sup>

The role of cellular structures, such as mitochondria and microtubules, in generating electromagnetic fields and biophotons remains a subject of ongoing investigation.<sup>25,29,30</sup> Our study contributes to this discussion, although further research is needed to fully understand these processes and their potential impact on cellular function.

The significance of our findings lies in the potential implications for understanding disease etiology and pathophysiology. If intercellular communication through electromagnetic fields holds true, it could revolutionize our approach to understanding and treating various diseases. This knowledge could have profound applications in biology and medicine, offering new perspectives on disease mechanisms and potential therapeutic avenues.

In conclusion, our study establishes a connection between biophoton emission, spatial cell arrangement, and oligospermia. We can gain valuable insights into the dynamics of cellular activity in response to disease by considering our assessment. Although our results challenge some significant notions, they offer possibilities for future biology and medicine research.

#### Acknowledgments

This work has been supported and performed at the Department of Biology and Anatomical Sciences, School of Medicine, Shahid Beheshti University of Medical Science. The present article is sponsored by "Laser Application in Medical Sciences Research Center, Shahid Beheshti University of Medical, Sciences, Tehran, Iran" (Registration No, 32110). In this regard, the authors wish to thank Dr. Hamed Shaker for improving the manuscript's writing on Ultraweak Photon Emission section.

#### Author's Contribution

**Conceptualization:** Mohammad-Amin Abdollahifar, Masoomeh Dashtdar.

**Data curation:** Mohammad-Amin Abdollahifar, Arefeh Aryan, Fakhroddin Aghajanzpour.

**Formal analysis:** Mohammad-Amin Abdollahifar, Arefeh Aryan, Fakhroddin Aghajanzpour.

**Funding acquisition:** Mohammad-Amin Abdollahifar.

**Investigation:** Mohammad-Amin Abdollahifar, Masoomeh Dashtdar, Arefeh Aryan, Fakhroddin Aghajanzpour.

**Methodology:** Mohammad-Amin Abdollahifar, Masoomeh Dashtdar, Fatemeh Fadaei Fathabadi.

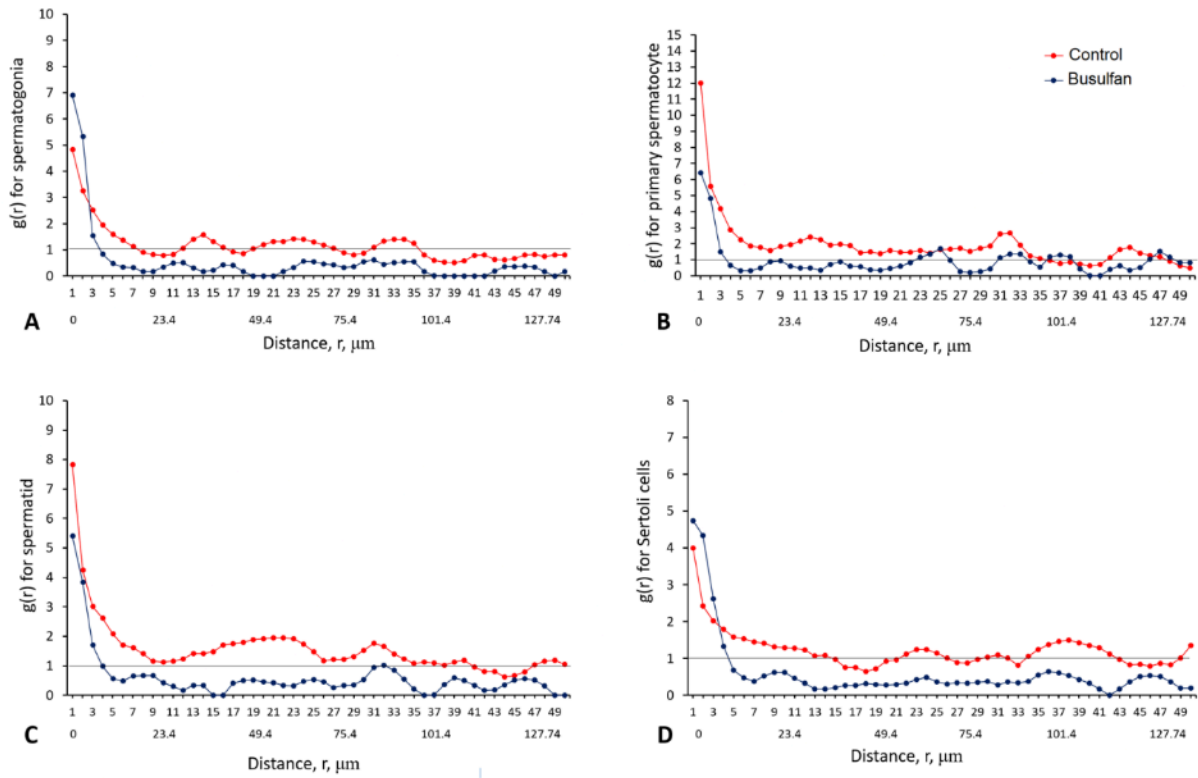
**Project administration:** Mohammad-Amin Abdollahifar.

**Resources:** Arefeh Aryan, Fakhroddin Aghajanzpour, Masoomeh Dashtdar, Fatemeh Hejazi, Maryam Salimi, Azar Afshar, Reza Soltani, Ahad Hasan Seyed Hasani, Abbas Aliaghaei, Hojjat-Allah Abbaszadeh, Hasan Mahmoodi, Leila Zahedi, Mohammad-Amin Abdollahifar, Fatemeh Fadaei Fathabadi.

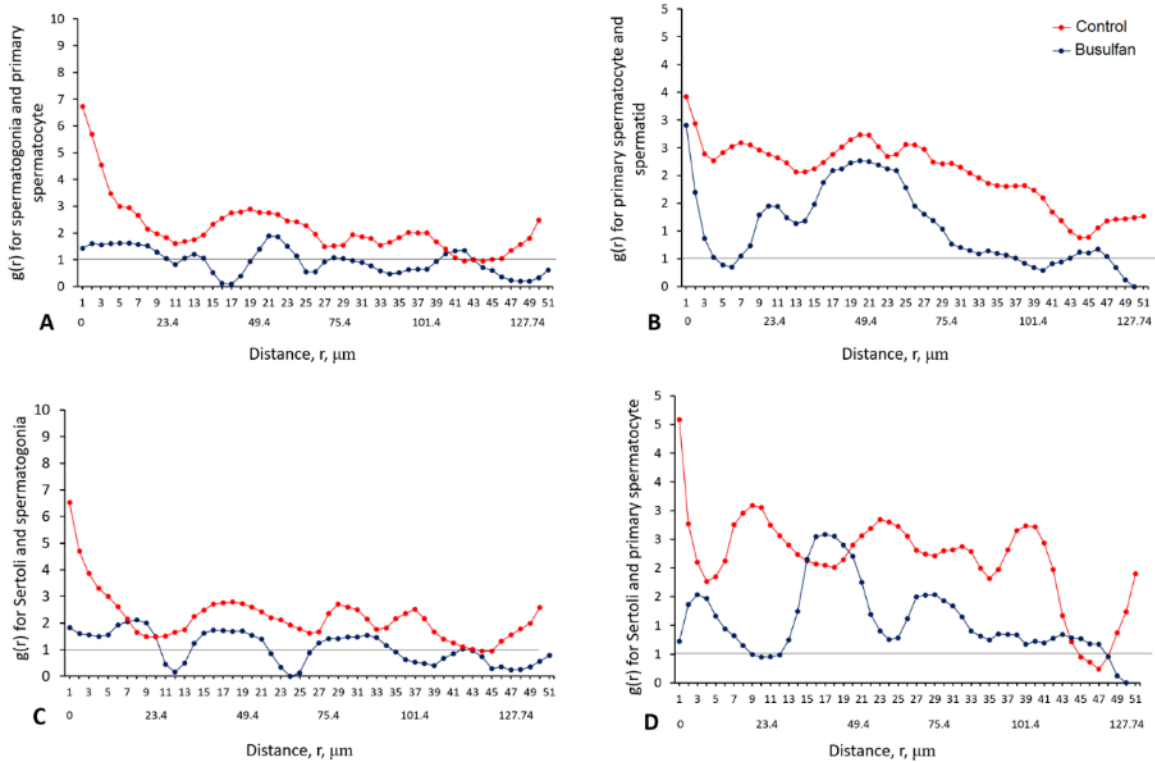
**Software:** Mohammad-Amin Abdollahifar, Masoomeh Dashtdar.

**Supervision:** Mohammad-Amin Abdollahifar, Fatemeh Fadaei Fathabadi.

**Validation:** Fatemeh Hejazi, Maryam Salimi, Azar Afshar, Reza Soltani, Ahad Hasan Seyed Hasani, Abbas Aliaghaei, Hojjat-Allah Abbaszadeh, Hasan Mahmoodi, Leila Zahedi.



Pair correlation functions



Cross correlation functions

**Figure 6.** Evaluation of the Spatial Arrangement of Testicular Cells Using the Second-Order Stereological Method. (A-D) Communication between pair-correlation function and cross-correlation functions of dipole distance for testicular cells in the study groups. The mean points are  $g(r)$  in the control and busulfan groups. The horizontal reference axis relates to values expected for a random spatial arrangement [ $g(r)=1$ ]





**Visualization:** Fatemeh Hejazi, Maryam Salimi, Azar Afshar, Reza Soltani, Ahad Hasan Seyed Hasani, Abbas Aliaghaei, Hojjat-Allah Abbaszadeh, Hasan Mahmoodi, Leila Zahedi.

**Writing–original draft:** Mohammad-Amin Abdollahifar, Fatemeh Fadaei Fathabadi.

**Writing–review & editing:** Arefeh Aryan, Fakhroddin Aghajanzour, Masoomeh Dashtdar, Fatemeh Hejazi, Maryam Salimi, Azar Afshar, Reza Soltani, Ahad Hasan Seyed Hasani, Abbas Aliaghaei, Hojjat-Allah Abbaszadeh, Hasan Mahmoodi, Leila Zahedi, Mohammad-Amin Abdollahifar, Fatemeh Fadaei Fathabadi.

#### Competing Interests

The authors declare that they have no competing interests.

#### Data Availability Statement

The data and materials supporting the findings of this study are available from the corresponding author upon reasonable request.

#### Ethical Approval

This study has been approved by the Medical Ethics Commission of Shahid Beheshti University of Medical Sciences, Tehran, Iran (IR.SBMU.MSP.REC. 1400.023).

#### Funding

The present article is sponsored by “Laser Application in Medical Sciences Research Center, Shahid Beheshti University of Medical Sciences, Tehran, Iran” (Registration No, 32110).

#### References

- Aronoff S. Plasmodesmata. *Science*. 1976;194(4261):176-7. doi: [10.1126/science.194.4261.176-a](https://doi.org/10.1126/science.194.4261.176-a).
- Kučera O, Cifra M. Cell-to-cell signaling through light: just a ghost of chance? *Cell Commun Signal*. 2013;11:87. doi: [10.1186/1478-811x-11-87](https://doi.org/10.1186/1478-811x-11-87).
- Bloemendal S, Kück U. Cell-to-cell communication in plants, animals, and fungi: a comparative review. *Naturwissenschaften*. 2013;100(1):3-19. doi: [10.1007/s00114-012-0988-z](https://doi.org/10.1007/s00114-012-0988-z).
- Du J, Deng T, Cao B, Wang Z, Yang M, Han J. The application and trend of ultra-weak photon emission in biology and medicine. *Front Chem*. 2023;11:1140128. doi: [10.3389/fchem.2023.1140128](https://doi.org/10.3389/fchem.2023.1140128).
- Lucas WJ, Ham BK, Kim JY. Plasmodesmata - bridging the gap between neighboring plant cells. *Trends Cell Biol*. 2009;19(10):495-503. doi: [10.1016/j.tcb.2009.07.003](https://doi.org/10.1016/j.tcb.2009.07.003).
- Sager RE, Lee JY. Plasmodesmata at a glance. *J Cell Sci*. 2018;131(11):jcs209346. doi: [10.1242/jcs.209346](https://doi.org/10.1242/jcs.209346).
- Madl P, Verwanger T, Geppert M, Scholkmann F. Oscillations of ultra-weak photon emission from cancer and non-cancer cells stressed by culture medium change and TNF- $\alpha$ . *Sci Rep*. 2017;7(1):11249. doi: [10.1038/s41598-017-10949-z](https://doi.org/10.1038/s41598-017-10949-z).
- Pospíšil P. Production of reactive oxygen species by photosystem II. *Biochim Biophys Acta*. 2009;1787(10):1151-60. doi: [10.1016/j.bbapoc.2009.05.005](https://doi.org/10.1016/j.bbapoc.2009.05.005).
- Prasad A, Pospíšil P. Towards the two-dimensional imaging of spontaneous ultra-weak photon emission from microbial, plant and animal cells. *Sci Rep*. 2013;3:1211. doi: [10.1038/srep01211](https://doi.org/10.1038/srep01211).
- Albrecht-Buehler G. Surface extensions of 3T3 cells towards distant infrared light sources. *J Cell Biol*. 1991;114(3):493-502. doi: [10.1083/jcb.114.3.493](https://doi.org/10.1083/jcb.114.3.493).
- Tsuchida K, Iwasa T, Kobayashi M. Imaging of ultraweak photon emission for evaluating the oxidative stress of human skin. *J Photochem Photobiol B*. 2019;198:111562. doi: [10.1016/j.jphotobiol.2019.111562](https://doi.org/10.1016/j.jphotobiol.2019.111562).
- Wu Q, Lu S, Zhang L, Zhao L. LncRNA HOXA-AS2 activates the notch pathway to promote cervical cancer cell proliferation and migration. *Reprod Sci*. 2021;28(10):3000-9. doi: [10.1007/s43032-021-00626-y](https://doi.org/10.1007/s43032-021-00626-y).
- Zapata F, Pastor-Ruiz V, Ortega-Ojeda F, Montalvo G, Ruiz-Zolle AV, García-Ruiz C. Human ultra-weak photon emission as non-invasive spectroscopic tool for diagnosis of internal states - a review. *J Photochem Photobiol B*. 2021;216:112141. doi: [10.1016/j.jphotobiol.2021.112141](https://doi.org/10.1016/j.jphotobiol.2021.112141).
- Reed MG, Howard CV, GS DEY. One-stop stereology: the estimation of 3D parameters using isotropic rulers. *J Microsc*. 2010;239(1):54-65. doi: [10.1111/j.1365-2818.2009.03356.x](https://doi.org/10.1111/j.1365-2818.2009.03356.x).
- Johnsen SG. Testicular biopsy score count—a method for registration of spermatogenesis in human testes: normal values and results in 335 hypogonadal males. *Hormones*. 1970;1(1):2-25. doi: [10.1159/000178170](https://doi.org/10.1159/000178170).
- Peirouvi T, Aliaghaei A, Eslami Farsani B, Ziaei-pour S, Ebrahimi V, Forozesh M, et al. COVID-19 disrupts the blood-testis barrier through the induction of inflammatory cytokines and disruption of junctional proteins. *Inflamm Res*. 2021;70(10-12):1165-75. doi: [10.1007/s00011-021-01497-4](https://doi.org/10.1007/s00011-021-01497-4).
- Mattfeldt T, Eckel S, Fleischer F, Schmidt V. Statistical analysis of reduced pair correlation functions of capillaries in the prostate gland. *J Microsc*. 2006;223(Pt 2):107-19. doi: [10.1111/j.1365-2818.2006.01604.x](https://doi.org/10.1111/j.1365-2818.2006.01604.x).
- Mayhew TM. Second-order stereology and ultrastructural examination of the spatial arrangements of tissue compartments within glomeruli of normal and diabetic kidneys. *J Microsc*. 1999;195(Pt2):87-95. doi: [10.1046/j.1365-2818.1999.00593.x](https://doi.org/10.1046/j.1365-2818.1999.00593.x).
- Sajadi E, Dadras S, Bayat M, Abdi S, Nazarian H, Ziaei-pour S, et al. Impaired spermatogenesis associated with changes in spatial arrangement of Sertoli and spermatogonial cells following induced diabetes. *J Cell Biochem*. 2019;120(10):17312-25. doi: [10.1002/jcb.28995](https://doi.org/10.1002/jcb.28995).
- Krasnoperov RA, Stoyan D. Second-order stereology of spatial fibre systems. *J Microsc*. 2004;216(Pt 2):156-64. doi: [10.1111/j.0022-2720.2004.01407.x](https://doi.org/10.1111/j.0022-2720.2004.01407.x).
- Ilkhani S, Moradi A, Aliaghaei A, Norouzian M, Abdi S, Rohjani E, et al. Spatial arrangement of testicular cells disrupted by transient scrotal hyperthermia and subsequent impairment of spermatogenesis. *Andrologia*. 2020;52(9):e13664. doi: [10.1111/and.13664](https://doi.org/10.1111/and.13664).
- Devaraj B, Kobayashi M, Takeda M, Ito H, Jin M, Inaba H. Detection and characterization of ultraweak biophotons from life processes. In: *Optical Methods in Biomedical and Environmental Sciences*. Amsterdam: Elsevier; 1994. p. 3-6.
- Cohen S, Popp FA. Whole-body counting of biophotons and its relation to biological rhythms. In: Chang JJ, Fisch J, Popp FA, eds. *Biophotons*. Dordrecht: Springer; 1998. p. 183-91. doi: [10.1007/978-94-017-0928-6\\_13](https://doi.org/10.1007/978-94-017-0928-6_13).
- Jung HH, Woo WM, Yang JM, Choi C, Lee J, Yoon G, et al. Left-right asymmetry of biophoton emission from hemiparesis patients. *Indian J Exp Biol*. 2003;41(5):452-6.
- Van Wijk R, Van Wijk EPA, Pang J, Yang M, Yan Y, Han J. Integrating ultra-weak photon emission analysis in mitochondrial research. *Front Physiol*. 2020;11:717. doi: [10.3389/fphys.2020.00717](https://doi.org/10.3389/fphys.2020.00717).
- Mordente A, Meucci E, Silvestrini A, Martorana GE, Giardina B. Anthracyclines and mitochondria. In: Scatena R, Bottoni



- P, Giardina B, eds. *Advances in Mitochondrial Medicine*. Dordrecht: Springer; 2012. p. 385-419. doi: [10.1007/978-94-007-2869-1\\_18](https://doi.org/10.1007/978-94-007-2869-1_18).
27. DeVita VT Jr, Chu E. A history of cancer chemotherapy. *Cancer Res*. 2008;68(21):8643-53. doi: [10.1158/0008-5472.can-07-6611](https://doi.org/10.1158/0008-5472.can-07-6611).
  28. Burger K, Mühl B, Harasim T, Rohrmoser M, Malamoussi A, Orban M, et al. Chemotherapeutic drugs inhibit ribosome biogenesis at various levels. *J Biol Chem*. 2010;285(16):12416-25. doi: [10.1074/jbc.M109.074211](https://doi.org/10.1074/jbc.M109.074211).
  29. Pokorný J, Jelínek F, Trkal V. Electric field around microtubules. *Bioelectrochem Bioenerg*. 1998;45(2):239-45. doi: [10.1016/s0302-4598\(98\)00100-7](https://doi.org/10.1016/s0302-4598(98)00100-7).
  30. Nan X, Sims PA, Chen P, Xie XS. Observation of individual microtubule motor steps in living cells with endocytosed quantum dots. *J Phys Chem B*. 2005;109(51):24220-4. doi: [10.1021/jp056360w](https://doi.org/10.1021/jp056360w).